Journal of Alloys and Compounds 739 (2018) 380–387

Contents lists available at ScienceDirect

Journal of Alloys and Compounds

journal homepage: http://www.elsevier.com/locate/jalcom

Investigation of $GaBi_{1-x}Sb_x$ based highly mismatched alloys: Potential thermoelectric materials for renewable energy devices and applications

S. AlFaify [a, **, 1], Bakhtiar Ul Haq [a, *, 1], R. Ahmed [b, c, ***], Faheem K. Butt [d, e], M.M. Alsardia [f]

[a] Advanced Functional Materials & Optoelectronics Laboratory (AFMOL), Department of Physics, Faculty of Science, King Khalid University, P.O. Box 9004, Abha, Saudi Arabia
[b] Department of Physics, Faculty of Science, Universiti Teknologi Malaysia, UTM, Skudai, 81310, Johor, Malaysia
[c] Centre for High Energy Physics, University of the Punjab, Quid-e-Azam Campus, Lahore, Pakistan
[d] Physik-Department ECS, Technische Universität München, Garching, Germany
[e] Department of Physics, Division of Science and Technology, University of Education, College Road, Township, Lahore, Pakistan
[f] Department of Physics, Sungkyunkwan University, Suwon, 440-746, Republic of Korea

ARTICLE INFO

Article history:
Received 4 June 2017
Received in revised form
11 December 2017
Accepted 25 December 2017
Available online 27 December 2017

Keywords:
Density functional theory
Electronic band structure
Seebeck coefficients
Power factor
Figure of merit

ABSTRACT

The high-performance thermoelectric materials are considered a potential resource for clean and sustainable energy. Highly mismatched alloys (HMAs), that are admired for the dramatic modifications in their electronic band structures can essentially play important role in developing high-performance thermoelectric materials. Here, we explore the potential of $GaBi_{1-x}Sb_x$ based HMAs for their thermoelectric applications via density functional theory coupled with the Boltzmann transport theory. To perform a comprehensive analysis, four different Sb alloying compositions such as GaBi, $GaBi_{0.875}Sb_{0.125}$, $GaBi_{0.75}Sb_{0.25}$, and $GaBi_{0.625}Sb_{0.375}$, are considered. It is found that the Sb replacement over Bi in $GaBi_{1-x}Sb_x$ has stimulated two major modifications in the electronic band structure: the band-gap enhancement, and contraction in the curvature of conduction band minimum. These features have remarkably evolved the thermoelectric properties of $GaBi_{1-x}Sb_x$ as a function of Sb contents. The significant increase in Seebeck coefficient and decrease in the electrical conductivity of $GaBi_{1-x}Sb_x$ alloy as a function of Sb content have resulted in large values of thermoelectric power factor as well as the figure of merit (ZT). Considerable improvement in the ZT values as a function of Sb has been recorded that approaches to ~1.0 for $GaBi_{0.625}Sb_{0.375}$ at room temperature. The occurrence of optimal thermoelectric coefficient values, at attainable doping levels below the Fermi level reveals the predominantly p-type nature of the $GaBi_{1-x}Sb_x$. Hence, $GaBi_{1-x}Sb_x$ ($GaBi_{0.625}Sb_{0.375}$ in particular) exhibits interesting thermoelectric properties at room temperature, and is therefore believed to be good candidate material for room temperature based thermoelectric devices and applications.

1. Introduction

The escalating increase in the environmental pollution due to the globalization, the industrial revolution and increased population demands for the alternative and renewable sources. Therefore researchers have shown a remarkable interest in the quest for finding new and improved methods and resources to bring clean, abundant and renewable sources of energy to the society in harmony with nature. This worldwide demand can be accomplished for example, by new and highly efficient energy generating devices based on materials that are earth-abundant and non-toxic. Such motives have made thermoelectrics one of the fascinating topics in the field of sustainable energy utilization [1,2]. The feature of direct inter-conversion between heat energy and electrical energy for

* Corresponding author.
** Corresponding author.
*** Corresponding author. Department of Physics, Faculty of Science, Universiti Teknologi Malaysia, UTM, Skudai, 81310, Johor, Malaysia.
E-mail addresses: saalfaify@kku.edu.sa (S. AlFaify), bakhtiar@kku.edu.sa (B. Ul Haq), rashidahmed@utm.my (R. Ahmed).
[1] These authors contributed equally.

https://doi.org/10.1016/j.jallcom.2017.12.306
0925-8388/

power generation or refrigeration reveals the significant potential of thermoelectric materials in solving the energy crises that likely can make essential contributions to reducing the carbon-based fuels and cutting energy waste [3]. The efficiency of these materials in terms of converting heat into electrical energy is characterized by the dimensionless figure of merit. The figure of merit, $ZT = S^2\sigma T/\kappa$ is determined by Seebeck coefficient (S), absolute temperature (T), electrical conductivity (σ), and thermal conductivity. To attain a high value of ZT, a large value of the Seebeck coefficient, high electrical conductivity, and low thermal conductivity are needed simultaneously. However, the conflicting correlation between these parameters is the major complexity in achieving the maximum ZT value. Maximizing the ZT value is, therefore, demanding for optimized values of a number of parameters such as carrier concentration, effective masses of charge carriers, and the electronic/lattice thermal conductivity that have been the subject of significant ongoing research in recent years.

Literature shows that relatively high ZT values materials, ranging from 0.6 to 1.1 (at 773–823 K), have been reproduced by employing different approaches such as doping [3,4], microstructure modulation [5,6] and band structure engineering via alloying [7,8]. Alloying of materials (semiconductors in particular) is a pronounced approach offering numerous opportunities for tailoring new dimensions into their physical properties for any desired applications [9–14]. Literature also illustrates that alloying has often been practiced among iso-electronic semiconductors holding relatively well-matching properties for achieving the characteristics as demanded for electronic and optoelectronic applications [10–17]. Such conventional alloys are typically represented by the relation $A_{(1-x)}B_{(x)}C$, where A and B represents the cations usually belongs to group-II or III elements and the anions C is taken from the corresponding VI or V. However, with swift advances in the fabrication and characterization techniques, a new trend of alloying has been established, where the alloying constituents are chosen to be highly mismatched in terms of their physical properties, and this novel class of materials is therefore named as a highly mismatched alloys (HMAs) [16,18–23]. They are now described by the relation $XY_{(1-x)}Z_{(x)}$, with X being the cation from II or III and, Y and Z are the corresponding anions. In contrast to conventional alloys, the host anions are replaced by elements that exhibit enhanced physical properties in HMAs. The capability of HMAs to bring in dramatic evolution in the physical properties, particularly the electronic band gap on account of minor compositional change has triggered the high interest of the scientific community. It is therefore believed that the capability of dramatic modifications in the electronic band structure of HMAs can possibly provide sufficient room for the enhanced thermoelectric performance.

Although many HMAs have been explored for the applications in electronics, optoelectronics, a deep understanding of their thermoelectric coefficients is scarce so far [14,24,25], that demands further investigations in order to develop a useful guide for enhancing their thermoelectric properties. In this paper, we attempted the designing of highly mismatched alloys (HMAs) based on $GaBi_{1-x}Sb_x$ with tunable band gap/band structure and subsequent modulation in thermoelectric properties. The aim of the present study is to examine the potential of the $GaBi_{1-x}Sb_x$ for thermoelectric applications in the framework of density functional theory in conjunction with the Boltzmann transport theory. To explore the dependence of thermoelectric properties $GaBi_{1-x}Sb_x$ on the alloying concentration and temperature, we looked into different compositions of these HMAs such as GaBi, $GaBi_{0.875}Sb_{0.125}$, $GaBi_{0.75}Sb_{0.25}$, and $GaBi_{0.625}Sb_{0.375}$, at 300 K, 600 K, and 900 K to this end.

1.1. Research methodology

In the present DFT based electronic structures study, the calculations are done by the full potential linearized-augmented-plus-local-orbital (FP-L(APW+lo)) method. The basis set used is therefore realized by dividing the unit cell into two regions namely: the interstitial region and the non-overlapping spheres centered on the atoms. In the interstitial region, the wave functions are represented by the plane wave basis set, where inside the spherical region, are augmented by the atomic-like wave function. The wave functions inside the spherical region (muffin-tin spheres) have been expanded up to $l_{max} = 10$, where for the convergence of eigenvalues in the interstitial region, energy cutoff $K_{max} = 8.0/R_{MT}$ (Ryd) $^{1/2}$ was taken into account. The electronic-structure related calculations are performed by the modified Becke-Johnson (mBJ) exchange potential [26–28] including the spin-orbit coupling (SOC) through the second variational procedure [29,30]. Different compositions of $GaBi_{1-x}Sb_x$ are realized by constructing so-called supercells with 16 atoms/cell. To achieve the ground state, geometry optimization was performed by relaxing the ionic positions and cell size. The R_{MT} values were chosen for Ga, Bi and Sb as 2.08 a.u, 2.30 a.u, and 2.30 a.u respectively. The Fourier-expanded charge density was truncated at $G_{max} = 16$ au^{-1}. The Brillion Zone (BZ) integration has been done using Monkhorst–Pack special k-points approach [31]. For good convergence of energy, the integrals over the special BZ are performed up to 256 ($8 \times 8 \times 8$) k-points. The total energy was found to be converged to 10^{-5}Ryd/unit cell in our present self-consistent computations for well-defined results. Calculations based on the mentioned computational details were executed by WIEN2k code [32].

The results of the electronic structure calculations have been used for the calculations of thermoelectric properties within a semiclassical Boltzmann theory under a constant scattering time approximation as implemented in the BoltzTraP code [33]. A brief summary of the adopted method for the calculations of electrical conductivity, Seebeck coefficient, power factor (PF), and ZT value has been given in the following, whereas a detailed explanation of the Boltzmann transport theory can be found elsewhere [34,35]. The mentioned thermoelectric coefficients have been determined as a function of chemical potential (μ) and temperature using the following equations.

$$\sigma_{\alpha\beta}(T,\mu) = \frac{1}{\Omega}\int \Sigma_{\alpha\beta}(\varepsilon)\left[-\frac{\partial f_0(T,\varepsilon,\mu)}{\partial\varepsilon}\right]d\varepsilon, \tag{1}$$

$$S_{\alpha\beta}(T,\mu) = \frac{1}{eT\Omega\sigma_{\alpha\beta}(T,\mu)}\int (\varepsilon-\mu)\Sigma_{\alpha\beta}(\varepsilon)\left[-\frac{\partial f_0(T,\varepsilon,\mu)}{\partial\varepsilon}\right]d\varepsilon, \tag{2}$$

where α and β are Cartesian indices of the tensor quantities. Symbols e, Ω and f_o represent the electronic charge, volume of the unit cell and the Fermi–Dirac distribution function of the carriers respectively.

The energy projected transport distribution function represented by $\Sigma_{\alpha\beta}$ is central term in equations (1) and (2) and can be defined as

$$\Sigma_{\alpha\beta}(\varepsilon) = \frac{e^2}{N}\sum_{i,k}\tau v_\alpha(i,k)v_\beta(i,k)\delta(\varepsilon-\varepsilon_{i,k}), \tag{3}$$

where $v_\alpha(i,k) = \frac{1}{\hbar}\frac{\partial\varepsilon_{i,k}}{\partial k_\alpha}$ represents the group velocity, and i, k, N, and τ mentioned in Eq. (3) are used for the band index, wave vector, the total number of k-points used for the BZ sampling and relaxation

time, respectively. Since the wave-vector-dependent relaxation time is an undetermined quantity in the present calculations, the τ-dependent quantities such as electrical conductivity and power factor ($S^2\sigma$) are reported with respect to τ i.e σ/τ and $S^2\sigma/\tau$.

2. Results and discussion

In the present DFT based investigations of the thermoelectric properties of $GaBi_{1-x}Sb_x$, four different compositions of Sb alloying such as GaBi, $GaBi_{0.875}Sb_{0.125}$, $GaBi_{0.75}Sb_{0.25}$, and $GaBi_{0.625}Sb_{0.375}$ are considered for a comprehensive understanding of composition induced modifications in the thermoelectric parameters. Fig. 1 shows a schematic of the designed 16-atoms supercell of GaBi used in the present study.

GaBi has been found to be thermodynamically stable in zinc-blende phase with the space groups of $F\overline{4}3m$ [36,37]. The lattice constant "*a*" of GaBi in zinc-blende phase has been estimated in experiments as 6.33 Å [38], whereas the first-principles based approaches report it as 6.28 Å [36], 6.26 [39], 6.324 Å [37]. GaBi demonstrates a lot of similarity with GaSb that crystalizes in zinc-blende phase with a lattice constant of magnitude ~6.10 Å [40], 6.12 Å [41]. This provides a good opportunity for the mutual alloying of GaBi and GaSb such as $GaBi_{1-x}Sb_x$. Moreover, the solubility of Sb at high concentration in the matrix of GaBi can be anticipated. Owing to these features, the alloying between the constituents of GaBi and GaSb (such as $GaBi_{1-x}Sb_x$) has been practiced in both experimental [42–48] and theoretical [49–51] frameworks.

Next, we examine the effect of Sb contents on the electronic band structure of $GaBi_{1-x}Sb_x$ as the modifications in the electronic band structure alter the electrical conductivity and consequently the other thermoelectric coefficients. Hence, we determine the density of states of $GaBi_{1-x}Sb_x$ against energy using mBJ+SOC (Fig. 2).

Fig. 2, shows that $GaBi_{1-x}Sb_x$ based HMAs possess noticeably narrow bandgap that however undergo a considerable enhancement with an increase in Sb contents. Our analysis of the electronic band structures reveals that Sb alloying with GaBi has induced two considerable modifications in the band structure. First is that; replacing Sb over Ga has affected the conduction band edges by pushing them to higher energies in the conduction band that grounds the observed increase in the band gap of $GaBi_{1-x}Sb_x$ as a function of Sb concentration. The advancement of the conduction band minimum (CBM) into upper conduction band as a function of Sb concentration has been shown in the inset of Fig. 2. Our analysis of the partial DOS (Fig. 3) shows that CBM of GaBi is defined mainly by the Ga related bands (*s*-band in particular) with some contribution from Bi related *s,p*-states. Alloying of Sb with GaBi

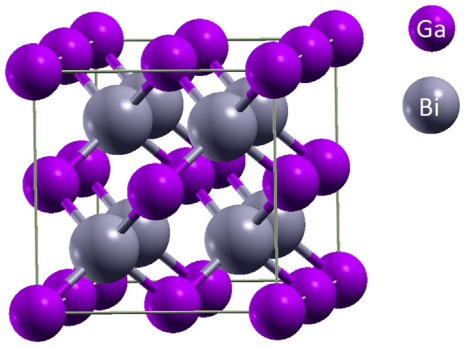

Fig. 1. Schematic of the designed 16-atoms supercell of GaBi used in the present study.

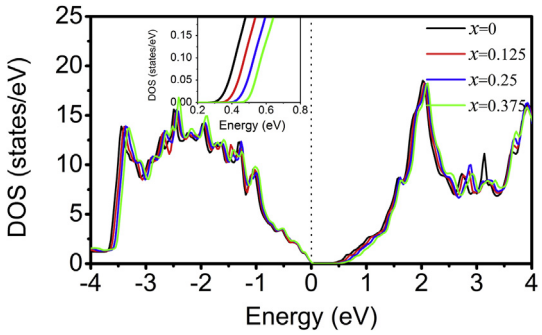

Fig. 2. Total density of states of $GaBi_{1-x}Sb_x$ for $x = 0$, 0.125, 0.25, and 0.375 determined with mBJ+SOC. The inset shows the upward movement of the conduction band minimum as a function of Sb concentration.

introduces Sb related impurity states into the valence and conduction bands in the vicinity of Fermi level. Although Sb related impurity bands experience strong hybridization with Bi-*p* in the valence band, their influence is rather significant in the lower part of the conduction band where the Sb-*s,p* states, mixed with Ga-*s* and Bi-*p*, lead to significant modifications in the arrangement of states in the lower conduction band. The upward movement of the conduction band is likely the result of the interactions taking place between these mixed states that consequently enhanced the energy band-gap. The dependence of energy band gap on the alloying composition has been shown in Fig. 4(a). The increase in the band gap on account of Sb content has also been reported concerning various other materials such as SnO_2 [52], $CuAlO_2$ [53], Bi_2Te_3 [54] and ZnO [55] etc.

The second major observation is regarding the parabolic bands defining the conduction band minimum where their curvatures experience a continuous reduction in their radii as the Sb concentration increases (Fig. 4(b)). The radii of the curvatures defined by the bandgap edges show significant influence on the masses of the charge carriers associated with these bands. The correlation between the curvatures of the band edges and masses of the charge carriers can be further understood by the following equation.

$$d^2E/dk^2 = \hbar^2/m \quad (4)$$

It is evident from equation (4) that bandgap edges with larger curvatures are conducive to heavier masses of charge carriers and vice versa. Consequently, heavier masses of charge carriers on account of larger curvature results in lowering the electrical conductivity of the corresponding solid materials.

Based on equation (4), we assume heavier masses of electrons in GaBi due to its comparatively larger CBM's curvature, however, GaBi simultaneously exhibits narrower band-gap, resulting in sufficiently larger electrical conductivity compared to the other alloying compositions. The effect of bandgap enhancement on the electrical conductivity is further seen in Fig. 5, where the conductivity of $GaBi_{1-x}Sb_x$ based HMA decreases with increase in Sb composition. Besides, the difference in the electronegativity values of the constituents of the $GaBi_{1-x}Sb_x$ also was found to be playing important role in the observed degradation of the electrical conductivity. In principle, a small difference in the electronegativities of the constituents is more favorable for covalent bonding and therefore results in higher carrier mobility [56], otherwise, the carrier mobility is lower. In the present case, the difference in the Pauling electronegativity of Ga (~1.81) with Sb (~2.05) is larger as compared to that of Bi (~2.02), as a result carrier mobility in GaBi is potentially larger than that of $GaBi_{0.875}Sb_{0.125}$, $GaBi_{0.75}Sb_{0.25}$, and $GaBi_{0.625}Sb_{0.375}$. Therefore, the decrease in the electrical

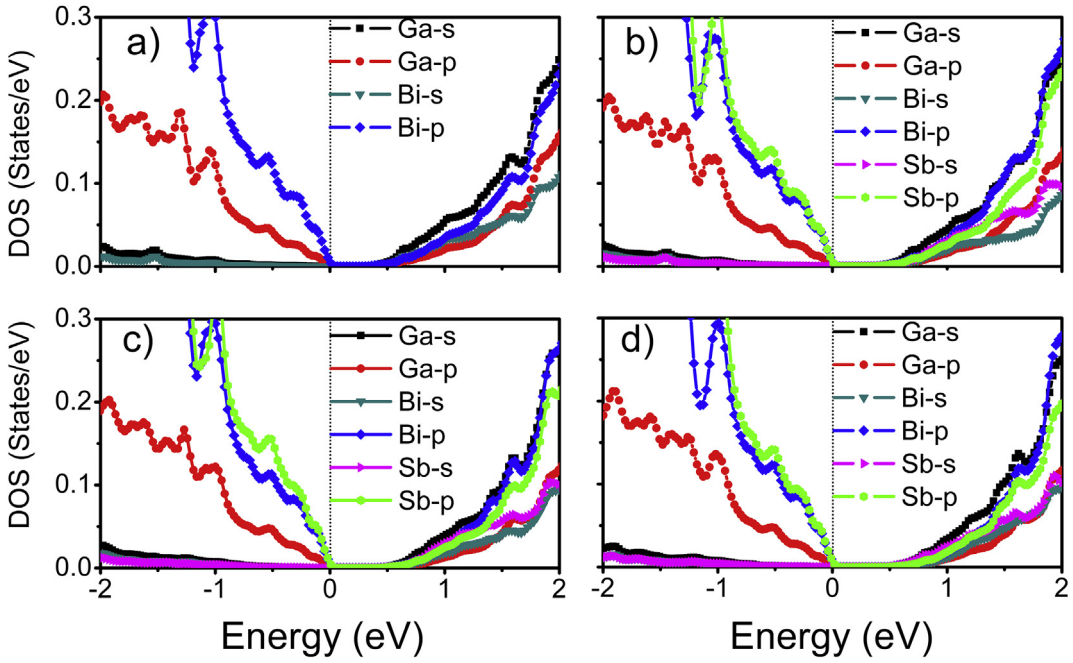

Fig. 3. The partial density of states of $GaBi_{1-x}$ Sb_x for $x = 0$ (a), 0.125 (b), 0.25 (b), and 0.375 (d) highlighting the role of Ga, Bi and Sb related s,p electrons into the electronic properties of $GaBi_{1-x}$ Sb_x.

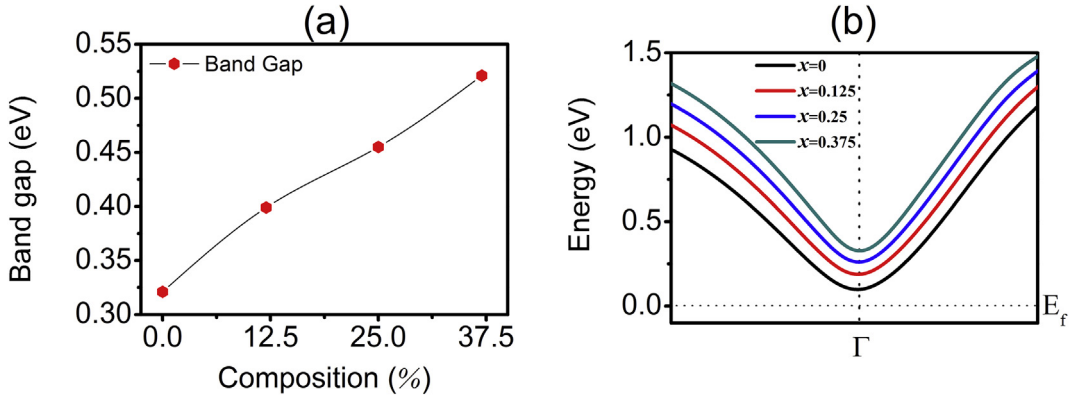

Fig. 4. **(a)** The enhancement in the energy gap of $GaBi_{1-x}$ Sb_x has been shown as a function of Sb concentration. **(b)**The dependence of conduction band minimum of $GaBi_{1-x}$ Sb_x along Γ-point in the Brillion zone. An obvious reduction in the radii of the curvature of the conduction band minimum has been seen as a function of Sb concentration.

conductivities of $GaBi_{1-x}Sb_x$ HMA with an increase of Sb contents can be attributed to the combined effect of enhanced energy bandgaps and the degradation in carrier mobility due to the difference of their electronegativities.

We further investigate the effect of temperature on the electrical conductivity of $GaBi_{1-x}Sb_x$ by performing calculations at three different temperatures such as 300 K, 600 K, and 900 K. Fig. 5, further demonstrates the effect of temperature on the electrical conductivity. The response of the electrical conductivity to the temperature is such that it increases monotonically with temperature, showing that $GaBi_{1-x}Sb_x$ based HMAs are semiconductor in nature. The electrical conductivity of GaBi at Fermi level was recorded as 4.53×10^{18}/Ωms at 300 K that increased to 0.05×10^{20}/Ωms at 600 K and 0.055×10^{20}/Ωms at 900 K. Whereas the electrical conductivity of $GaBi_{0.875}Sb_{0.125}$ magnitudes to 3.15×10^{11}/Ωms at 300 K, 1.06×10^{15}/Ωms at 600 K and 2.09×10^{16}/Ωms at 900 K, for $GaBi_{0.75}Sb_{0.25}$, the calculated conductivity at Fermi level was found as 5.09×10^{9}/Ωms at 300 K, 1.41×10^{14}/Ωms at 600 K and 6.19×10^{15}/Ωms at 900 K and for $GaBi_{0.625}Sb_{0.375}$, the electrical conductivity amounts to 2.53×10^{9}/Ωms at 300 K, 1.03×10^{14}/Ωms at 600 K and 5.11×10^{15}/Ωms at 900 K. As can be seen from Fig. 5, the electrical conductivity experiences an abrupt increase in the vicinity of Fermi level corresponding to the band gap edges.

As seen, the pure GaBi exhibits sufficiently larger electrical conductivity over Fermi level due to its narrower band gap and a large number of charge carriers. However, the electrical conductivity of GaBi experiences rapid reduction upon Sb substitution. This reduction in the electrical conductivity can be attributed to the enchantment of energy gaps and reduction in carrier's mobility for the replacement of Sb over Bi. The reduction in electrical conductivity is likely to stimulate significant enhancement in the Seebeck coefficients and ZT values. However, the variation in the electrical conductivity is relatively less significant among $GaBi_{0.875}Sb_{0.125}$, $GaBi_{0.75}Sb_{0.25}$, and $GaBi_{73.5}Sb_{62.5}$. As a result, the variation in the transport coefficients is predicted less significant with an increase in Sb compositions in $GaBi_{0.875}Sb_{0.125}$, $GaBi_{0.75}Sb_{0.25}$, and

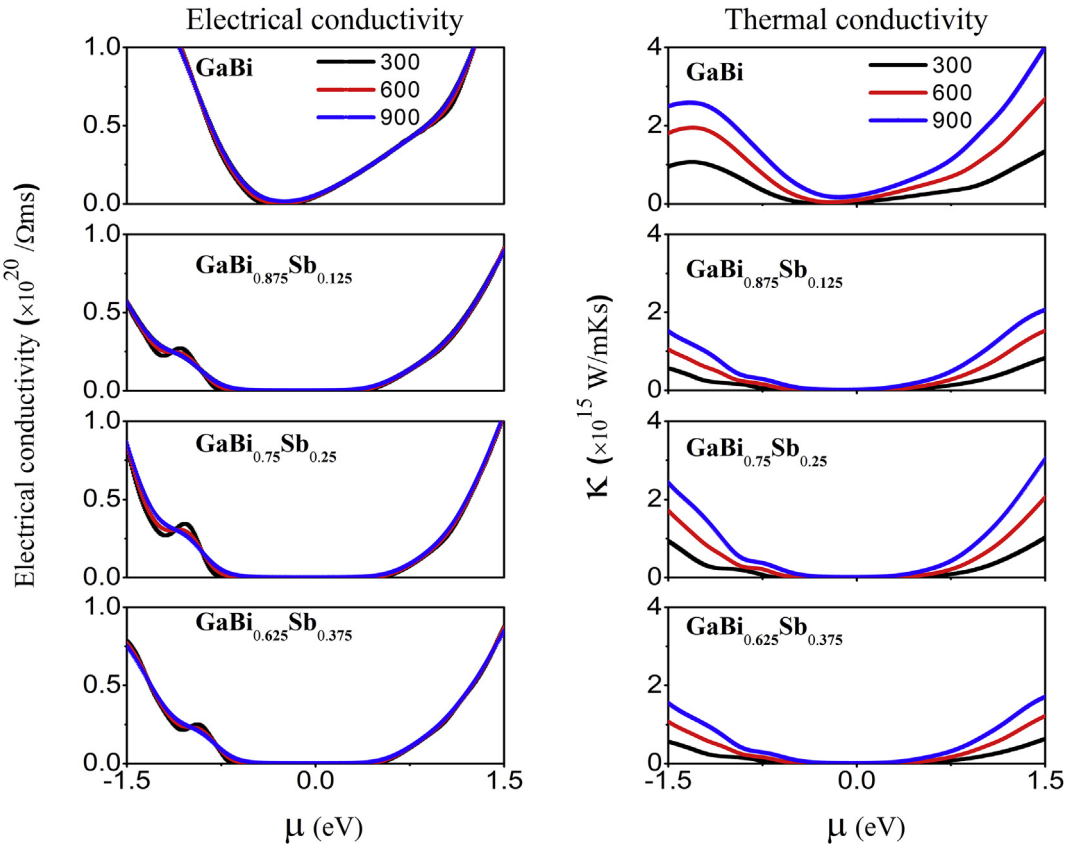

Fig. 5. Dependence of electrical conductivity (σ/τ) and thermal conductivity (κ) of $GaBi_{1-x}Sb_x$ based HMAs for $x = 0$, 0.125, 0.25, and 0.375 on chemical potential and temperature. The σ/τ and κ are found to increase to with temperature due to semiconducting nature of $GaBi_{1-x}Sb_x$.

$GaBi_{73.5}Sb_{62.5}$.

In addition to electrical conductivities, the thermal conductivities of the considered compositions of $GaBi_{1-x}Sb_x$ have also been calculated as shown in Fig. 5. It is seen that the increase in thermal conductivity of $GaBi_{1-x}Sb_x$ with an increase in temperature is significant than that of electrical conductivity. In the adopted Boltzmann transport theory for thermoelectric calculations, the thermal conductivity is majorly considered from the contribution of the electrons whereas the role of lattice thermal conductivity is neglected [33]. This is sufficiently reasonable as increase in temperature (particularly above room temperature) leads to the excitations of electrons that consequently result in the enhancement of electrical thermal conductivity. Whereas the sever lattice vibration with increase in temperature results in enhancing the ratio of phonon scattering that subsequently reduces lattice contributions to the thermal conductivity [57]. This inverse relation of lattice thermal conductivity with temperature has also been reported in experiments [58]. Thus it is reasonable to assume the insignificant contribution from lattice thermal conductivity to the total thermal conductivity in comparison with the electronic contribution at high temperature. Therefore the adopted approach is believed to provide a sufficiently good estimate of thermal conductivity and thermoelectric figure of merit at room temperature and above.

Our analysis shows that the electrical and thermal conductivities of $GaBi_{1-x}Sb_x$ have larger values for n-type doping or electrons than p-type or holes possibly due to the lighter masses of electrons in CB than holes in VB.

On the other hand, the Seebeck coefficients of $GaBi_{1-x}Sb_x$ shown in Fig. 6, occur with optimal values for p-type doping as it is proportional to holes concentration ($p^{-2/3}$). The electrical

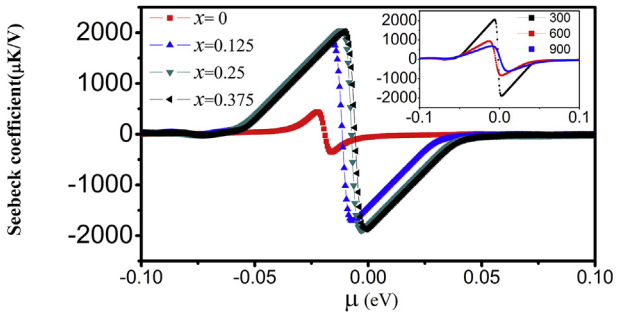

Fig. 6. Modifications in the Seebeck coefficient (S) of $GaBi_{1-x}Sb_x$ based HMAs for $x = 0$, 0.125, 0.25, and 0.375 on the account of Sb contents. Seebeck coefficients experience an abrupt increase in the presence of Sb. Seebeck coefficients of $GaBi_{1-x}Sb_x$ were found to decrease with increase in temperature. In the inset, a prototype temperature dependence of Seebeck coefficient has been shown for $GaBi_{0.75}Sb_{0.25}$.

conductivities encounter for the mentioned range of energy with minimum value due to their inverse relation with Seebeck coefficients. It is, therefore, GaBi exhibit a comparatively lower Seebeck coefficient for its calculated higher electrical conductivity. Hence, our results are fairly consistent with each other. The typical appearance of Seebeck coefficients below the Fermi level suggests that p-type doping is more favorable for $GaBi_{1-x}Sb_x$ alloys.

At room temperature, GaBi exhibits its maximum Seebeck value of magnitude 438.5 μV/K at −0.27 eV and −354.0 μV/K at −0.22 eV. However, a dramatic increase in the Seebeck value $GaBi_{1-x}Sb_x$ has been observed in the presence of Sb contents. For instance, the Seebeck coefficient of $GaBi_{0.875}Sb_{0.125}$ is almost four times larger

than that of GaBi. $GaBi_{0.875}Sb_{0.125}$ attains maximum Seebeck value of magnitude 1860 μV/K at - 0.22 eV and 1710 μV/K at −0.10 eV respectively. Similarly, for the $GaBi_{0.75}Sb_{0.25}$, Seebeck value has been recorded as 2050 μV/K at −0.15 eV and 1890 μV/K at −0.04 eV, whereas $GaBi_{0.625}Sb_{0.375}$ attains maximum values of Seebeck coefficients at −0.14 eV and −0.014 eV of magnitude 2080 μV/K and −1893 μV/K respectively.

The Seebeck coefficient plays important role in the thermoelectric performance of any material. A typical value of 150–250 μV/K or greater is considered a prerequisite to achieve the demanded value of ZT (≈ 1) for good thermoelectric performance [59]. Therefore $GaBi_{1-x}Sb_x$ alloys with high Seebeck values proficiently fulfill the fundamental requirement for thermoelectric applications. In fact, these alloys possess the Seebeck values comparable to that of the well-recognized thermoelectric materials such as PbTe [60,61]. The Seebeck coefficient of $GaBi_{1-x}Sb_x$ calculated in the present study experiences significant reduction with an increase in temperature. A prototype of Seebeck coefficient's dependence on temperature has been shown in the inset of Fig. 6.

The major structures appear in the electrical conductivity and Seebeck coefficient stem the PF ($S^2\sigma/\tau$) at the corresponding energies. Hence the peaks appear in the PF might be originated from a corresponding peak either in the electrical conductivity, Seebeck coefficients or both. The calculated maximum values of PF with corresponding energies are listed in Table 1. We recorded large PF in GaBi of magnitude 8.34×10^{14}μW/cmK^{2}s for n-type doping at 0.75 eV (Fig. 7). Since the Seebeck coefficient has negligible value at the corresponding energy, the PF is therefore assumed to be mainly contributed by the high electrical conductivity of magnitude 0.76×10^{20}/Ωms at the corresponding chemical potential. In contrast to GaBi, the PF favors p-type doping in the case of $GaBi_{0.875}Sb_{0.125}$, $GaBi_{0.75}Sb_{0.25}$, and $GaBi_{73.5}Sb_{62.5}$, and go through significant improvement in the presence of Sb contents. The maximum PF value in the case of $GaBi_{0.875}Sb_{0.125}$, $GaBi_{0.75}Sb_{0.25}$, and $GaBi_{0.625}Sb_{0.375}$ is considered being the joint contribution of electrical conductivity and Seebeck coefficient as both parameters exhibit noteworthy response at the corresponding energies. The maximum value of PF for $GaBi_{0.875}Sb_{0.125}$ described by sharp peak magnitudes to ~12. 38×10^{14}μW/cmK^{2}s at −0.75 eV. The recorded electrical conductivity and Seebeck coefficients at this energy amounts to 0.033×10^{20}/Ωms and 191.7 μV/K respectively. For $GaBi_{0.75}Sb_{0.25}$, the PF achieves maximum value of magnitude ~12.40×10^{14}μW/cmK^{2}s at −0.82 eV with electrical conductivity ~0.064×10^{20}/Ωms and Seebeck value 151.4 μV/K at the corresponding energy. Similarly, the maximum PF for $GaBi_{0.625}Sb_{0.375}$ magnitudes to 12.41×10^{14} μW/cmK^{2}s at −0.72 eV, and the corresponding electrical conductivity and Seebeck coefficients were recorded as ~0.037×10^{20}/Ωms and 183.70 μV/K respectively. The high values of PF of $GaBi_{1-x}Sb_x$ emphasize the capacity of these materials to quantify the actual electrical power produced by a temperature gradient. Although no literature is available on the thermoelectric properties of $GaBi_{1-x}Sb_x$ to our knowledge, our results are fairly comparable to the thermoelectric properties of narrow bandgap materials comprising of heavy atoms such as PbTe

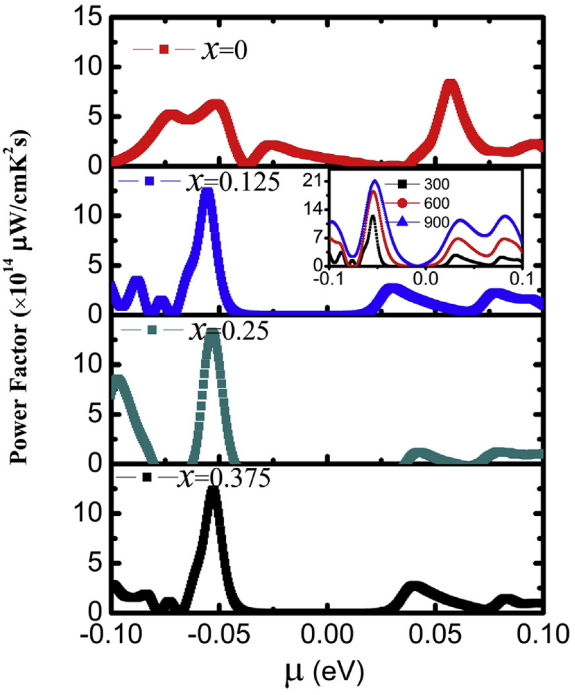

Fig. 7. The thermoelectric power factors of $GaBi_{1-x}Sb_x$ based HMAs for $x = 0$, 0.125, 0.25, and 0.375 on the account of Sb contents have been shown. A significant evolution has been seen in the power factors $GaBi_{1-x}Sb_x$ in the presence of Sb contents. Further increase in the power factor values has been recorded with an increase in temperature as shown in the inset for $GaBi_{0.875}Sb_{0.125}$.

(~74×10^{14}μW/cmK^{2}s), YPtBi (~18×10^{14}μW/cmK^{2}s), Na3Bi (~7.5×10^{14}μW/cmK^{2}s), and TaAs (~53×10^{14}μW/cmK^{2}s) [60,61]. The response of the PF of $GaBi_{1-x}Sb_x$ alloys to the temperature is such that; it observes a linear increase with increasing temperature (See inset in Fig. 6). Our analysis shows that an increase of 300 K causes enhancement of order 1.5 to 2 in the PF.

The trade-off observed between the electrical conductivities and Seebeck coefficients of $GaBi_{1-x}Sb_x$ alloys propose the existence of an optimal doping level where the figure of merit ZT can attain a maximum value. These parameters are inter-related to each other by the following relation

$$ZT = \frac{S^2\sigma T}{\kappa} \tag{5}$$

In equation (5), κ represents the thermal conductivity. Furthermore, equation (5), suggests that ZT can be enhanced by lowering thermal conductivity, and enhancing the combined effect of the Seebeck coefficient and electrical conductivity. Fig. 8, shows dependence of ZT on Sb content and temperature with respect to chemical potential. The optimal ZT values occur at modest doping levels for all compositions of the investigated alloys, and favors p-type doping. As seen from figure, the ZT experiences a notable

Table 1
The maximum values of PF (in units of 10^{14}μW/cmK^{2}s) at room temperature with a position on energy window relative to Fermi level. The electrical conductivity (in units of 10^{20}/Ωms) and Seebeck coefficients (in units of μV/K) at energies corresponding to the maximum PF are also given. The concurrence of PF_{max} at positive energy is referred to n-type doping and vice versa.

Composition (x)	Type of doping	E_{peak}(eV)	PF_{max}(at 300K)	Electrical conductivity	Seebeck coefficients	ZT (at 300 K)
GaBi	n	0.75	8.34	0.76	−3.47	0.844,
$GaBi_{0.875}Sb_{0.125}$	p	−0.75	12.40	0.033	191.7	0.993
$GaBi_{0.75}Sb_{0.25}$	p	−0.82	12.40	0.064	151.4	0.994
$GaBi_{0.625}Sb_{0.375}$	p	−0.72	12.41	0.037	183.70	1.0

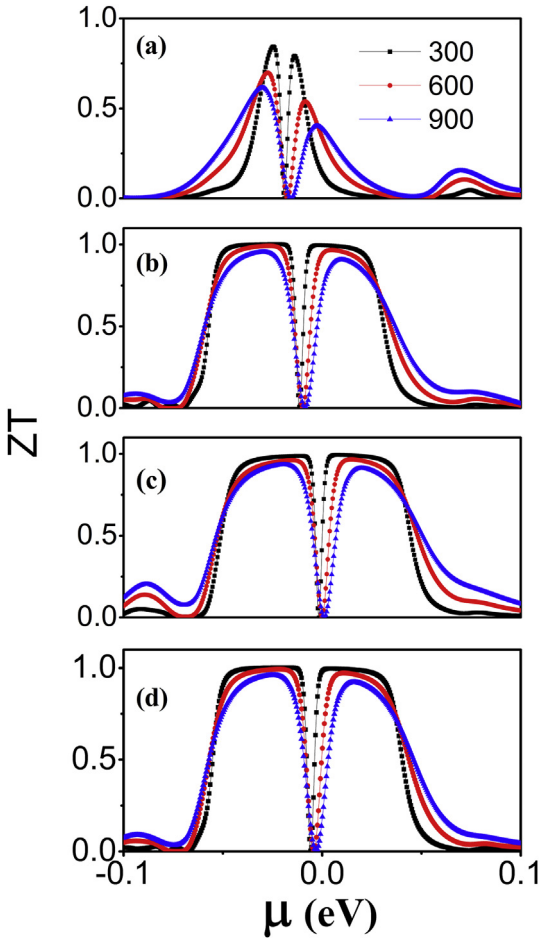

Fig. 8. The thermoelectric figure of merit (ZT) calculated for GaBi1$_{-x}$Sb$_x$ based HMAs for $x = 0$ (a), 0.125 (b), 0.25 (c), and 0.375 (d) as a function of temperature and Sb concentration. The ZT values of GaBi$_{1-x}$Sb$_x$ are considerably enhanced with an increase in Sb concentration. Moreover, ZT values have been degraded with an increase in temperature possibly due to the significant reduction was seen in the Seebeck coefficient.

increase in the presence of Sb content compared to GaBi. The room temperature ZT values for GaBi, GaBi$_{0.875}$Sb$_{0.125}$, GaBi$_{0.75}$Sb$_{0.25}$ have been listed in Table 1. The higher ZT values of GaBi$_{1-x}$Sb$_x$ alloys reveal them highly efficient for energy conversion at room temperature. The abrupt increase in ZT values is likely induced by the degraded electrical conductivities and enhanced Seebeck coefficients as a function of Sb content. Furthermore, the linear decrease in ZT with increase in temperature seen in Fig. 8, is possibly caused by the drastic reduction in Seebeck value with temperature (Fig. 5). The effect of electrical conductivity is ruled out as the change in electrical conductivity is comparatively less significant. Overall, the GaBi$_{1-x}$Sb$_x$ based highly mismatched alloys are predominantly p-type in nature where their thermoelectric coefficients with optimal values occur at attainable doping levels. It is therefore believed that they can be good candidates for thermoelectric applications.

3. Conclusions

In our present study, two foremost variations; 1) linear enhancement in the energy gap, 2) contraction of the curvature of conduction band minimum, in the electronic structures of the highly mismatched alloys GaBi$_{1-x}$Sb$_x$, were identified. Consequently, appealing results for thermoelectric properties like large values of Seebeck coefficients, thermoelectric power factors, and ZT ≈ 1 values, in particular, for GaBi$_{0.625}$Sb$_{0.375}$, at room temperature, were obtained. Moreover, the highly mismatched GaBi$_{1-x}$Sb$_x$ alloys were predominantly found in p-type nature and the values of their optimal parameters were found at attainable doping levels. Hence, the striking values of the thermoelectric figure of merit at room temperature and other features predict the GaBi$_{1-x}$Sb$_x$ alloys an appropriate candidate for the conversion of heat energy into electricity, in other words, this also predicts them as potential materials for thermoelectric applications that should be explored experimentally.

Acknowledgments

The authors extend their appreciation to the Deanship of Scientific Research at King Khalid University for funding this work through General Research Project under grant number (G.R.P-371-38).

References

[1] L.E. Bell, Cooling, heating, generating power, and recovering waste heat with thermoelectric systems, Science 321 (5895) (2008) 1457–1461.
[2] G.J. Snyder, E.S. Toberer, Complex thermoelectric materials, Nat. Mater. 7 (2) (2008) 105–114.
[3] T.-R. Wei, et al., Distinct impact of alkali-ion doping on electrical transport properties of thermoelectric p-type polycrystalline SnSe, J. Am. Chem. Soc. 138 (28) (2016) 8875–8882.
[4] E.K. Chere, et al., Studies on thermoelectric figure of merit of Na-doped p-type polycrystalline SnSe, J. Mater. Chem. A 4 (5) (2016) 1848–1854.
[5] Y. Fu, et al., Enhanced thermoelectric performance in p-type polycrystalline SnSe benefiting from texture modulation, J. Mater. Chem. C 4 (6) (2016) 1201–1207.
[6] S. Popuri, et al., Large thermoelectric power factors and impact of texturing on the thermal conductivity in polycrystalline SnSe, J. Mater. Chem. C 4 (8) (2016) 1685–1691.
[7] Y.-M. Han, et al., Thermoelectric performance of SnS and SnS–SnSe solid solution, J. Mater. Chem. A 3 (8) (2015) 4555–4559.
[8] T.-R. Wei, et al., Thermoelectric transport properties of pristine and Na-doped SnSe 1– x Te x polycrystals, Phys. Chem. Chem. Phys. 17 (44) (2015) 30102–30109.
[9] L. Xie, Two-dimensional transition metal dichalcogenide alloys: preparation, characterization and applications, Nanoscale 7 (44) (2015) 18392–18401.
[10] B.U. Haq, et al., Mutual alloying of XAs (X= Ga, In, Al) materials: tuning the optoelectronic and thermodynamic properties for solar energy applications, Sol. Energy 100 (2014) 1–8.
[11] B.U. Haq, R. Ahmed, S. Goumri-Said, DFT characterization of cadmium doped zinc oxide for photovoltaic and solar cell applications, Sol. Energy Mater. Sol. Cell. 130 (2014) 6–14.
[12] B.U. Haq, et al., Study of wurtzite and zincblende GaN/InN based solar cells alloys: first-principles investigation within the improved modified Becke–Johnson potential, Sol. Energy 107 (2014) 543–552.
[13] B.U. Haq, et al., Engineering of highly mismatched alloy with semiconductor and semi-metallic substituent's for photovoltaic applications, Curr. Appl. Phys. 17 (2) (2017) 162–168.
[14] B.U. Haq, et al., Composition-induced influence on the electronic band structure, optical and thermoelectric coefficients of the highly mismatched GaNSb alloy over the entire range: a DFT analysis, J. Alloys Compd. 693 (2017) 1020–1027.
[15] I. Vurgaftman, J. Meyer, L. Ram-Mohan, Band parameters for III–V compound semiconductors and their alloys, J. Appl. Phys. 89 (11) (2001) 5815–5875.
[16] F. Bernardini, V. Fiorentini, Nonlinear behavior of spontaneous and piezoelectric polarization in III-V nitride alloys, Phys. Status Solidi(a) 190 (1) (2002) 65–73.
[17] B. Jusserand, D. Paquet, F. Mollot, Dispersive character of optical phonons in GaAlAs alloys from Raman scattering in superlattices, Phys. Rev. Lett. 63 (21) (1989) 2397.
[18] W. Shan, et al., Band anticrossing in III-NV alloys, Phys. Status Solidi B Basic Res. 223 (1) (2001) 75–85.
[19] K. Alberi, et al., Valence band anticrossing in GaBixAs1– x, Appl. Phys. Lett. 91 (5) (2007) 051909.
[20] K. Alberi, et al., Valence-band anticrossing in mismatched III-V semiconductor alloys, Phys. Rev. B 75 (4) (2007) 045203.
[21] H. Baaziz, et al., Structural and electronic properties of GaN x As1– x alloys, Appl. Phys. A 106 (3) (2012) 687–696.
[22] D. Madouri, et al., Bismuth alloying in GaAs: a first-principles study, Comput. Mater. Sci. 43 (4) (2008) 818–822.

[23] M. Mbarki, A. Rebey, First-principles calculation of the physical properties of GaAs1-xBix alloys, Semicond. Sci. Technol. 26 (10) (2011) 105020.
[24] A. Reshak, Thermoelectric properties of highly-mismatched alloys of GaN x As 1− x from first-to second-principles methods: energy conversion, RSC Adv. 6 (76) (2016) 72286–72294.
[25] S.A. Khan, S. Azam, O. Sipr, Interrelationship between structural, optical and transport properties of InP 1− x Bix: DFT approach, Mater. Sci. Semicond. Process. 41 (2016) 45–53.
[26] F. Tran, P. Blaha, Accurate band gaps of semiconductors and insulators with a semilocal exchange-correlation potential, Phys. Rev. Lett. 102 (22) (2009) 226401.
[27] D. Koller, F. Tran, P. Blaha, Improving the modified Becke-Johnson exchange potential, Phys. Rev. B 85 (15) (2012) 155109.
[28] S. Azam, S.A. Khan, S. Goumri-Said, Modified Becke–Johnson (mBJ) exchange potential investigations of the optoelectronic structure of the quaternary diamond-like semiconductors Li 2 CdGeS 4 and Li 2 CdSnS 4, Mater. Sci. Semicond. Process. 39 (2015) 606–613.
[29] A. MacDonald, W. Picket, D. Koelling, A linearised relativistic augmented-plane-wave method utilising approximate pure spin basis functions, J. Phys. C Solid State Phys. 13 (14) (1980) 2675.
[30] P. Novak, et al., Electronic structure of the mixed valence system (Y M) 2 BaNiO 5 (M= Ca, Sr), Phys. Rev. B 63 (23) (2001) 235114.
[31] H.J. Monkhorst, J.D. Pack, Special points for Brillouin-zone integrations, Phys. Rev. B 13 (12) (1976) 5188.
[32] P. Blaha, et al., wien2k. An Augmented Plane Wave+ Local Orbitals Program for Calculating Crystal Properties, 2001.
[33] G.K. Madsen, D.J. Singh, BoltzTraP. A code for calculating band-structure dependent quantities, Comput. Phys. Commun. 175 (1) (2006) 67–71.
[34] B.R. Nag, Electron Transport in Compound Semiconductors, vol. 11, Springer Science & Business Media, 2012.
[35] T. Scheidemantel, et al., Transport coefficients from first-principles calculations, Phys. Rev. B 68 (12) (2003) 125210.
[36] M. Ferhat, A. Zaoui, Structural and electronic properties of III-V bismuth compounds, Phys. Rev. B 73 (11) (2006) 115107.
[37] A. Janotti, S.-H. Wei, S. Zhang, Theoretical study of the effects of isovalent coalloying of Bi and N in GaAs, Phys. Rev. B 65 (11) (2002) 115203.
[38] S. Tixier, et al., Molecular beam epitaxy growth of GaAs 1− x Bi x, Appl. Phys. Lett. 82 (14) (2003) 2245–2247.
[39] N.A.A. Rahim, et al., Computational modeling and characterization of X–Bi (X= B, Al, Ga, In) compounds: prospective optoelectronic materials for infrared/near infra applications, Comput. Mater. Sci. 114 (2016) 40–46.
[40] M. Straumanis, C. Kim, Lattice parameters, thermal expansion coefficients, phase width, and perfection of the structure of GaSb and InSb, J. Appl. Phys. 36 (12) (1965) 3822–3825.
[41] I. Remediakis, E. Kaxiras, Band-structure calculations for semiconductors within generalized-density-functional theory, Phys. Rev. B 59 (8) (1999) 5536.
[42] J. Kopaczek, et al., Low-and high-energy photoluminescence from GaSb1− xBix with 0< x≤ 0.042, Appl. Phys. Express 7 (11) (2014) 111202.
[43] M.K. Rajpalke, et al., Growth and properties of GaSbBi alloys, Appl. Phys. Lett. 103 (14) (2013) 142106.
[44] S. Das, et al., Near infrared photoluminescence observed in dilute GaSbBi alloys grown by liquid phase epitaxy, Infrared Phys. Technol. 55 (1) (2012) 156–160.
[45] M.K. Rajpalke, et al., High Bi content GaSbBi alloys, J. Appl. Phys. 116 (4) (2014) 043511.
[46] M.K. Rajpalke, et al., Bi flux-dependent MBE growth of GaSbBi alloys, J. Cryst. Growth 425 (2015) 241–244.
[47] S. Wang, Y. Song, I.S. Roy, Bismuth incorporation and lattice contraction in GaSbBi and InSbBi, in: Transparent Optical Networks (ICTON), 2011 13th International Conference on, IEEE, 2011.
[48] D. Samajdar, S. Dhar, Transport of bismuth atoms during liquid phase epitaxial growth of InSbBi and GaSbBi, Semicond. Sci. Technol. 28 (6) (2013) 065007.
[49] D. Samajdar, S. Dhar, Influence of Bi-related impurity states on the bandgap and spin–orbit splitting energy of dilute III–V-Bi alloys: InP 1− x Bi x, InAs 1− x Bi x, InSb 1− x Bi x and GaSb 1− x Bi x, Superlattices Microstruct. 89 (2016) 112–119.
[50] R. Alaya, M. Mbarki, A. Rebey, Pressure and composition dependence of structural, electronic and optical properties of GaAsBi alloys, Mater. Sci. Semicond. Process. 40 (2015) 925–930.
[51] M. Polak, et al., Theoretical and experimental studies of electronic band structure for GaSb1− xBix in the dilute Bi regime, J. Phys. D Appl. Phys. 47 (35) (2014) 355107.
[52] S. Gupta, et al., Microstructural, optical and electrical investigations of Sb-SnO 2 thin films deposited by spray pyrolysis, Mater. Res. Bull. 48 (9) (2013) 3315–3322.
[53] C. Ghosh, et al., Sb-doped CuAlO2: widening of band gap and nonlinear J–E characteristics, J. Mater. Sci. 46 (6) (2011) 1613–1621.
[54] B. Ryu, et al., Prediction of the band structures of Bi2Te3-related binary and Sb/Se-doped ternary thermoelectric materials, J. Kor. Phys. Soc. 68 (1) (2016) 115–120.
[55] P. Nakarungsee, et al., Sb substitution into ZnO nano-composite: ferromagnetic behavior, J. Magn. Magn. Mater. 397 (2016) 79–85.
[56] D.S. Lee, et al., Crystal structure, properties and nanostructuring of a new layered chalcogenide semiconductor, Bi 2 MnTe 4, CrystEngComm 15 (27) (2013) 5532–5538.
[57] Y.H.R. Chang, et al., Thermoelectric and piezoelectric properties of the predicted Al x In 1− x N composites based on ab initio calculations, Phys. Chem. Chem. Phys. 19 (36) (2017) 24613–24625.
[58] S. Ohta, et al., High-temperature carrier transport and thermoelectric properties of heavily La-or Nb-doped Sr Ti O 3 single crystals, J. Appl. Phys. 97 (3) (2005) 034106.
[59] T.M. Tritt, Thermoelectric phenomena, materials, and applications, Annu. Rev. Mater. Res. 41 (2011) 433–448.
[60] K. Pal, S. Anand, U.V. Waghmare, Thermoelectric properties of materials with nontrivial electronic topology, J. Mater. Chem. C 3 (46) (2015) 12130–12139.
[61] D.J. Singh, Doping-dependent thermopower of PbTe from Boltzmann transport calculations, Phys. Rev. B 81 (19) (2010) 195217.